2 Directional Xenon Measurement

3 ABSTRACT: Abstract...

Contents

1 Introduction

The use of Noble-liquid detectors in the field of astroparticle physics has increased in the past decades. Detectors aiming at measuring Dark Matter (DM) particles and neutrinos properties use large liquid argon or liquid xenon (LXe) chambers [1, 2]. Current and future experiment for DM detectioin are tuned to detect weakly interacting massive particles (WIMPs), a postulated candiadte for DM particle [3]. LXe based detectors are to date the leading in sensitivity and size for these searches [4–7].

When a particle interacts within the LXe media, it forms a cloud of excited and ionized states with typical length of 100 nm. The excited Xe (Xe^*) combines with other Xe atoms to form an excited dimer state (excimer) when they decay to ground state they emit light.

$$Xe^* + Xe \rightarrow Xe_2^* \rightarrow 2Xe + h\nu, \tag{1.1}$$
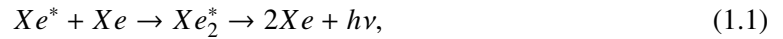
The electrons emitted from the ionization can recombine with a surrounding atom, this process of recombination provides another possibility to produce excimers,

$$
\begin{aligned}
Xe^+ + Xe &\rightarrow Xe_2^+ \\
Xe_2^+ + e^- &\rightarrow Xe^{**} \\
Xe^{**} &\rightarrow Xe^* + heat.
\end{aligned}
\tag{1.2}
$$

Once Xe^* is produced it adds to the scintillation process explained in 1.1. There are two types of Xe_2^* excimer states, singlet and triplet, with lifetime of $\sim$ 3 ns and $\sim$ 25 ns respectively. The wavelength emitted by these states is between (175-180) nm which is lower then the lowest excitation of xenon, and therefore travel through it to reach a photo-detector situated outside the LXe. Although much is measured on these scintillation processes, the basic knowledge of the quantum properties of these interactions is based on experiments preformed several decades ago.

The phenomenon of supperradiance in which identical quantum states "communicate" through electromagnetic field if in close proximity, is well studied. In certain conditions the emission of photons from these correlated states is very different then the sum of random states. This difference is in spectral, temporal and spatial properties [8, 9]. Early studies show that scintillation in LXe can produce coherent amplification of light [10, 11]. These studies were focusing on the macroscopic ionization using high energy density electron beams.

The understanding and quantification of the microscopic effects of non linear phenomena such as supperradiance in Lxe for a single interaction, can improve DM experiments to reduce background by the extra knowledge of directionality. irreducible background such as coherent neutrino nucleus scattering of neutrinos from the sun can be discard.

In this paper we present an experimental set-up called DIREXENO (Dirextional Xenon) aiming at measuring the spatial distribution of LXe scintillation light, and quantify non-isotropic emission.

2 Experimental Setup

The experimental setup that is described in this section, is designed to measure, the spatial and temporal properties of LXe scintillation. However it is designed in a modular way, so it can serve different requirements from different future experiments.

There are four main building blocks constructing the full setup, a schematics of them with the interfaces connecting them is shown in Fig. 1. The gas handling system, which, in normal working mode, drives the xenon from the detector trough a purifier and back into the detector. The cryogenic system, which liquefies the xenon and delivers it to the detector part. The detector system, mainly an HPFS sphere with a small bubble of LXe inside it surrounded with PMTs. Finally the data acquisition (DAQ) system that supplies HV and reads the data from all sensors (e.g., PMTs, pressure gauge etc.). Each building block can be replaced without effecting the others.

The full assembly (Fig. 2) is held on three separate racks, one for the DAQ, while the two others hold the cryogenic detector and gas handling system are joined using a 100mm bar with shock absorbers on both sides. Some of the guidelines for the design of DIREXENO are based on [12]

2.1 Gas handling system

A typical LXe detector must keep a high level of purity. Careful selection and meticulously cleaning of all parts before mounting, is needed, however is not sufficient. The desired level of most detectors of impurity concentration is at the level of 1 ppb O_2 equivalent [1]. This is crucial to allow ionization electrons drift for several cm. To reach that level in a reasonable amount of time
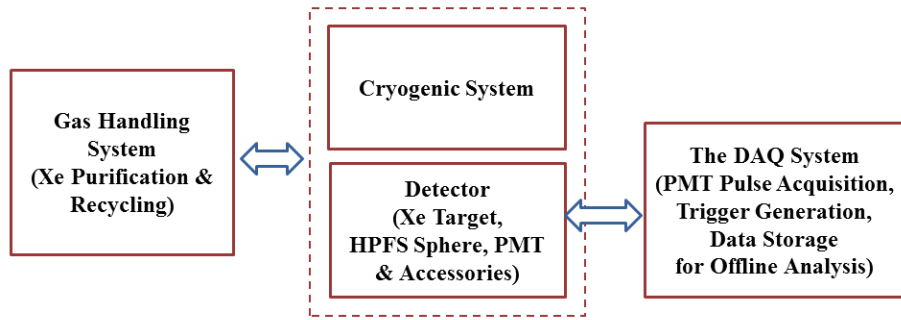
Figure 1. A schematic of DIREXENO showing all the four building blocks of the system.
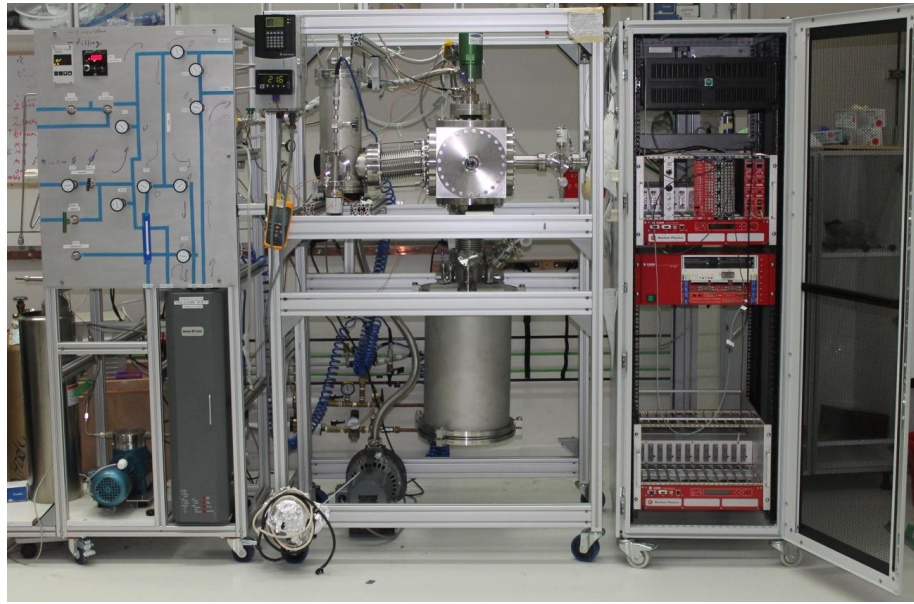

Figure 2. DIREXENO. On the left the purification system, in the middle the cryogenic and detector chamber, and on th right the Data acquisition system.

(several days instead of months), continuous purification is needed. The gas handling system, provides this process, alongside with all gas handling operations such as filling and recuperation.

During purification mode, xenon is taken from the chamber (in liquid phase) passes through a heat exchanger[1] where it is heated and vapored. The xenon is forced by a KNF diaphragm pump into a hot getter[2] which cleans the xenon from most impurities. The xenon also passes through an MKS Mass Flow Controller[3] (MFC), this allows monitoring and controlling the amount of xenon in the system.

After the xenon is purified, it is delivered back to the cryogenic system through the heat exchanger, there the remained xenon gas is liquefied before it continuous back to the chamber. A

---

[1]GEA GBS100M-24 plate heat exchanger
[2]MONO-TORR PS4-MT15-R-2
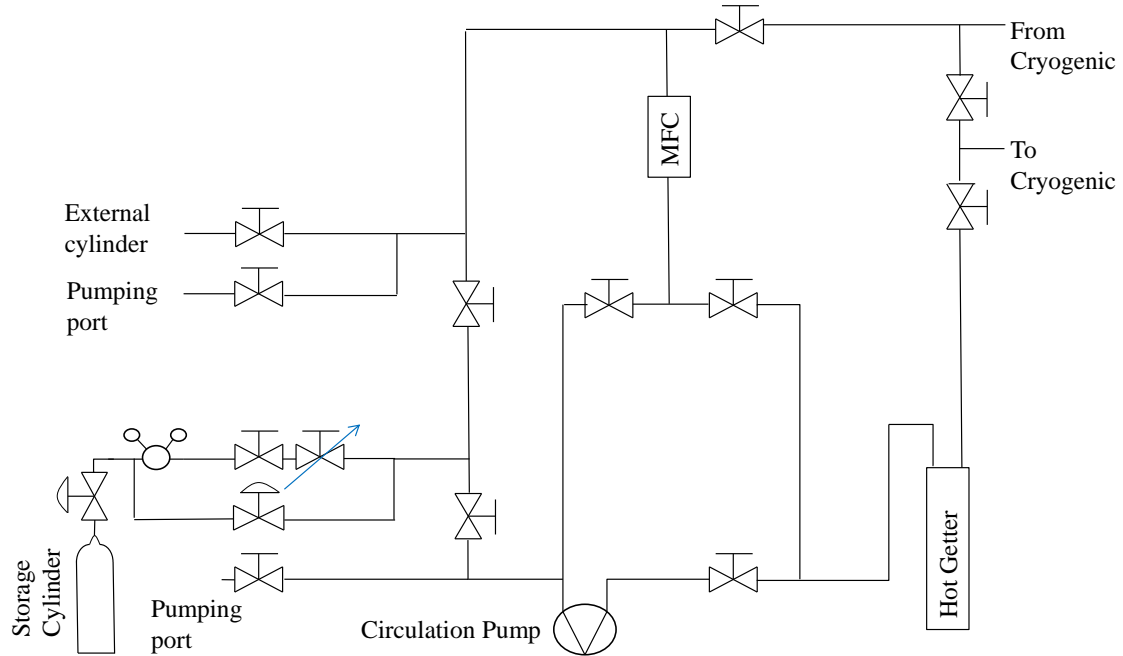[3]MKS mass flow controller

Figure 3. Schematics of the purification system. High pressure valves are indicated as valves with arcs. Needle valves are indicated as a valve with an arrow.

schematic of this system is shown in fig. 3.

2.2 Cryogenic system

Remote cooling is generally used in DM experiments due to background radiating from the cooler to the detector. Although in our system this is not of great importance there are still several advantages to remote cooling such as: lowering acoustic noise from the cryo-cooler and flexibility to design changes. The cryogenic system is connected on one side to the gas system and on the other to the detector chamber, any change in the system (e.g, cooler type or model) requires the change of that specific part without changing the detector nor the gas system.

The system is made out of two chambers, the outer vessel (OV) which holds the insulation vacuum, and the inner vessel (IV) that holds the xenon. In addition to the vacuum which prevents heat leaks from diffusion and convection, the entire IV is covered by multi layer aluminized Myler to prevent heating via radiation an image of the detector and the CAD design are shown in Fig 4.

The OV is made of a 10" CF cube, with ports on all six faces (e.g., FT, pumping ports, view ports). This vacuum is shared with the detector one via a 6" CF flexible bellows.

The IV is made of 1.5" height cylinder with 6" CF flanges on the top and bottom parts of it, and it holds inside xenon. A 120 mm diameter cold finger is welded to the top flange of the IV.
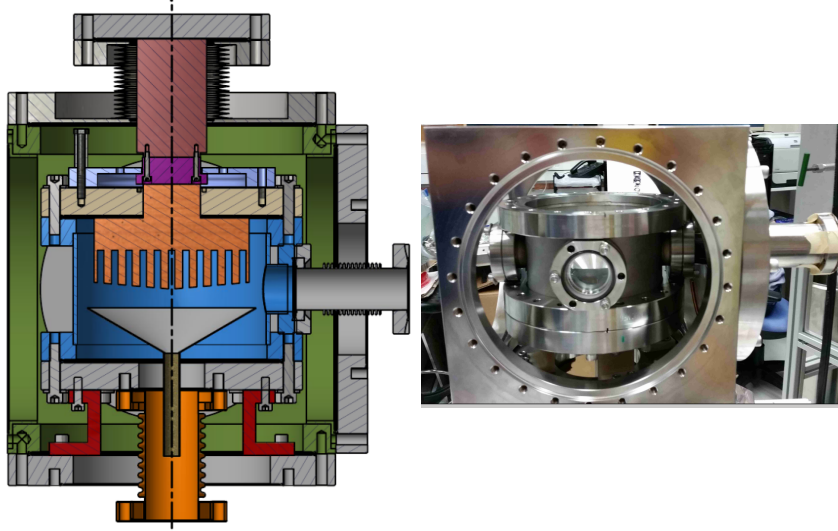
Figure 4. CAD view of the cryogenic system(Left) and a pictue of the cryogenic system (Right) .

The design of the cold finger is similar to the design of [13], the inner part of the cold finger is made of long fins, therefore the surface area of it is bigger resulting in a better heat transport. The upper part of the cold finger is in thermal contact with the cryo-cooler [1] via a cooper adapter. The copper adapter holds two 100Ω pt resistor which are connected to a PID reader[2] for temperature measurements. A Cartridge-heater is also inserted to the copper adapter for emergency heating.

The cryo-cooler provides up to 70 W of cooling power, and is connected via a $4\frac{1}{2}$" flange to the OV top flange, and reaching the IV top flange. Common cryo-coolers used for xenon experiments, work in maximal cooling mode permanently. The QDrive, instead, has temperature control allowing it vary the cooling power, which enables to set the temperature with fluctuations smaller then 0.1 C° on the cooler itself.

On the inner side of the bottom flange of the IV a thin SS funnel is installed collecting all LXe drops from the cold finger, and delivering them to the detector part. This flange is connected to the detector part, via a $3\frac{3}{8}$" flexible bellows. This bellows hosts two small pipes connected to the circulation system, and a third pipe coming from the funnel, all three pipes deliver LXe whereas the GXe is filling the bellows. The separation between the LXe coming from the gas handling system (clean) and the LXe coming from the cold finger (more dirty) allows the filling of clean LXe to different parts of the detector.

2.3   The Detector

The detector refers to the chamber and its inner assembly that contains the liquid Xenon bubble, the photomultiplier detectors around it and their accessories. This chamber is placed below the cryogenic system. We describe the detector chamber and its interface to the cryogenic system in section 2.3.1. In section 2.3.2 we discuss the assembly that consists of the HPFS sphere to hold liquid Xenon and the Photomultiplier detectors distributed around the sphere.

---

[1]QDrive 20BB 9p6 A 3 AYNBNCO
[2]cryo-con model 18i Cryogenic Temp Monitor

2.3.1 The Detector Chamber

The detector chamber is built such that apart from the interface to the cryogenic system, it can be changed and modified easily for future experiments. The interface unit is built out of 2 flanges welded together via 7 tubes, which serve as service ports for electrical and other feedthroughs. The upper flange, ISO-K NW320, is part of the OV and shares the insulation vacuum of the cryogenic system, the bottom one , CF-8", is part of an IV for future detectors, and would hold xenon inside. For our experiment we modified the CF flange to fit also a $4\frac{5}{8}$" CF flange which we use.

The OV is closed with a cylinder XXX cm height closed from the bottom with another ISO-K NW320 flange, the height of the cylinder is determined such that the maximal height of the whole apparatus is 190 cm, allowing the mobility of the detector through standard doors.

The $4\frac{5}{8}$" CF flange is connected to a closed vessel internally divided into two parts. This vessel serves as a xenon reservoir. The two parts of the vessel are connected to a spherical orb from above (inner part) and from below (outer part). LXe is circulated such that new LXe drips into the outer part and pumped from the inner one. This way the liquid level is controlled, and the sphere itself is always filled with LXe.

2.3.2 The Sphere

The central component of the detector assembly is the hollow sphere which holds the LXe target bubble. A spherical shell made of high purity fused silica with high transmittance is designed to hold the LXe target. The xenon will be circulated Two invar tubes are connected to it from the top and bottom with SS mini-CF flanges at the end, to circulate the xenon (see Fig.~6). The bottom flange of the sphere is held using a brass holder to prevent force or torque applied on the sphere while mounting the detector. The brass holder is connected to a plate held from the top 8" flange, and is also used to align this plate at first installation. A set of 20 PMTs[1] are placed around the sphere to detect light emitted from the LXe.

The LXe target bubble should not be too large in order to avoid double scatters. This shell should be large enough to reduce internal reflections, but not too large which would attenuate the scintillation light. The material of the shell should have a refractive index similar to LXe in order to have minimal diffraction from the original direction of the photons when they travel from the LXe target to the sphere. We chose corning HPFS 8655 as the shell material. The refractive index of HPFS 8655 is 1.575 at 185 nm (LXe R.I. 1.61). In Fig. 5, are the refractive indices at various wavelegths as given by the HPFS factsheet and also a naive extrapolation at lower wavelengths which are relevant to us.

The transmittance of the material is extremely crucial for us to optimize the dimension of the shell. Therefore, we obtained a 6 mm thick sample of HPFS 8655 and performed a transmittance testing a VUV monochromator setup. A deuterium light source was used to generate a spectrum in the range (110 - 950) nm, peaked approximately at 160 nm. The window of the light source faced a vacuum space pumped to below 10^{-4} Torr. The monochromator allows to select the desired wavelengths using a manually rotatable holographic diffraction grating. A PMT placed in the vacuum measured the intensity of light emitted from the monochromator, with and without the fused silica sample. The ratio of measured intensities was used to calculate the transmittance of
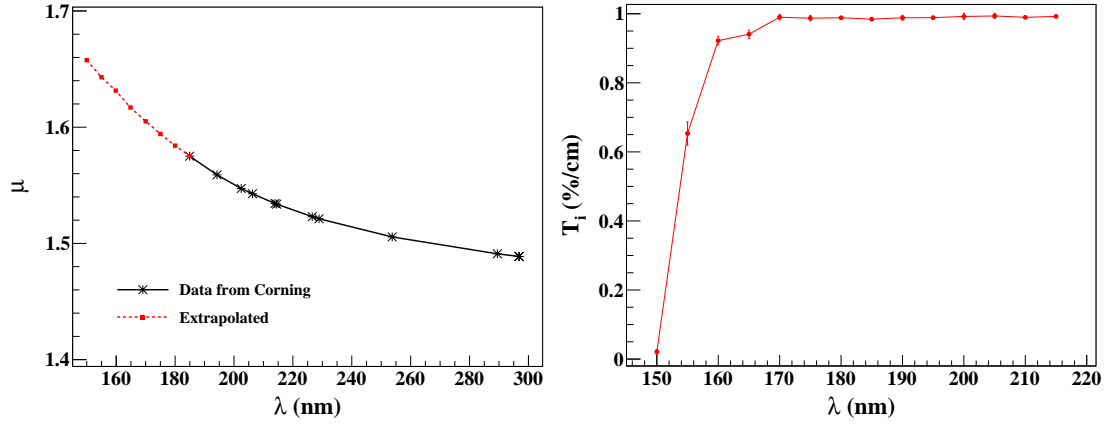
---

[1]r8520-406 Hamamatsu 1" PMT

Figure 5. The important characteristics of HPFS-8655. (Left) The refractive index as provided by corning and extrapolated to relevant wavelength range. (Right) The internal transmittance (T_i).
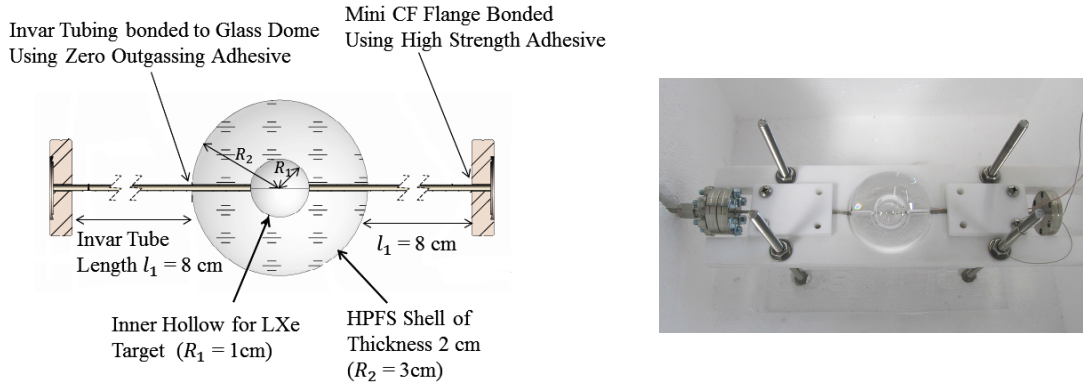

Figure 6. The technical design of the HPFS shell with invar tubing and flanges (left). The industrially manufactured HPFS shell (right).

the material. In fig. **??** is the measured transmittances/ 6 mm at (150 - 215) nm. At 175 nm the sample shows approximately 90%/6mm measured transmittance which corresponds to an intrinsic transmittance of about 98%.

The dimension of the fused silica shell is optimized by studying the path of the scintillation photons using a GEANT4 based simulation [14]. The sources that will be used for exciting the xenon, and creating the supperradiance (signal) as well as the standard emission (background), will be ^{137}Cs (662 keV) and ^{57}Co(122keV & 136 keV) for ER and ^{241}AmBe , D-D neutron generator, or neutron produced in an accelerator for NR . The mean free path for this energy is a couple of mm (^{57}Co) and (0.5 - 3) cm (^{137}Cs). We discuss the simulation in detail in section 4. The outer radius of the shell is 3 cm, while the inner radius of the hollow space that will hold the LXe is 1 cm. The flow of the LXe will be maintained by two invar tubes. In Fig. 6 we show the technical design and a picture of the industrially manufactured shell assebmly.

The photons coming out of the system will be detected by twenty 1" square Hamamatsu R8520-406 photomultiplier tubes with an active area of 20.5 mm × 20.5 mm each. We pick PMTs
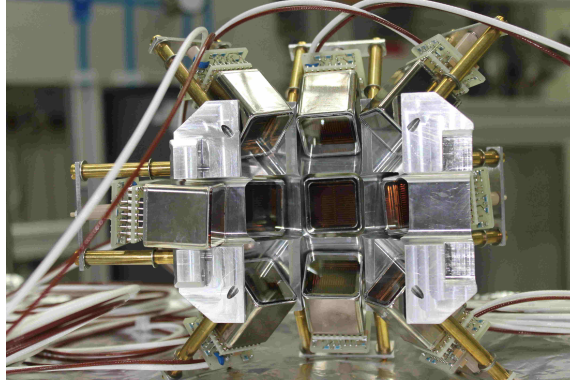
Figure 7. A PMT holder–hemisphere. We use two such components to hold 20 PMTS around the target.
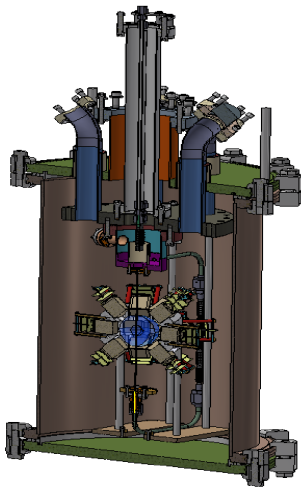

Figure 8. (Left) CAD design of the detector part. (Right) First mounting of the detector part, still not connected to the rest of the system.

with a minimum quantum efficiency of 30% at 178 nm. For an applied voltage of 900 V the gain of these PMTs are 2×10^6. We use a positive voltage divider, also manufactured by Hamamatsu, to provide high voltage to the PMTs. These 20 PMTs are held with a special aluminum holder, coated with anti-reflection substance. The holder is made of two hemispheres hosting the PMTs in 3 rows all of them pointing to the center of the fused-silica sphere. the PMTs are held only via their voltage–divider bases. The bases are held using M2 PEEK screws. In Fig. 7, one of the holder–hemispheres with the PMTs are shown.

In Fig. 8 we present a CAD schematic as well as a real view of the detector part.

3 The Data Acquisition (DAQ) System

[**MMD:** This part is almost complete, trigger logic details might get changed slightly]

In this section we discuss the data acquisition and readout from the PMT channels. We use a heterogeneous system consisting of both NIM and VME electronics modules, with the data readout

being carried out through the VME controller module V2718 and a PCIe card A3818.

The schematic layout of the DAQ system is shown in Fig. 9. All the 20 PMTs are oriented in the holder assembly which was discussed in section 2.3.2. The PMTs are ramped up to +800V (the maximum is +900V) using a 24 channel VME high volatge distributor module [1]. We define the raw electrical pulse output of the PMTs as Si (raw), where $i = 1 - 20$. These raw pulses are then amplified and shaped using two photomultiplier preamplifiers [2]. The preamplifier channels operates from DC to 275 MHz and produce two identical 50 Ω non inverting outputs with voltage gains of 10. We define the amplified pulses as Si, ($i = 1 - 20$). One out of the two identical analog outputs from each channel is converted to a digital signal with an Analog to Digitizer converter [3].

The ADC consists of two 12bit 5GS/s Switched capacitor Digitizer sections, each of them with 16+1 channels, based on DRS4 chip. The dynamic range of the input signal is 1 Vpp with adjustable DC offset. This module can sample either bipolar or unipolar analog input signal within the dynamic range in a circular analog memory buffer, with default sampling frequency choices 5GS/s, 2.5 GS/s or 2 GS/s. As soon as a trigger signal reaches, all the analog memory buffers gets frozen and then gets digitized into a digital memory buffer with a 12 bit resolution.

We generate an intrinsic trigger for the system, with the coincidence of any two out of the twenty PMTs. The second output from the preamplifier channels are converted to binary signals using two 16 channel leading Edge discriminator [4]. In Fig. 9, we term the binary outputs from the discriminator as SDi, i= $1 - 20$. The SDi signals are then passed over to the logic module [5] to obtain the trigger. At present, the coincidence of any two out of the twenty PMTs forms the trigger logic. The output of the logic operation is used to trigger the ADC. In order to record the PMT noise rate, the SDi signals are duplicated and fed to a scaler [6].

The PMT event information and the trigger rate are read from the ADC, while the Scaler records the PMT noise rate. The data readout to the acquisition PC is done through the Controller and optical link to the master PCIe card. The further analyses of the relevant events in the PMTs will be carried out offline using an analysis framework.

---

[1] iseg VDS18130p

[2] Phillips 776. Each of the preamplifier model provides 16 independent and direct-coupled amplifiers channels

[3] CAEN ADC V1742: Switched capacitor Digitizer

[4] CAEN V895

[5] CAEN V1495, an FPGA based General purpose VME board which is programmed to perform the logic operation
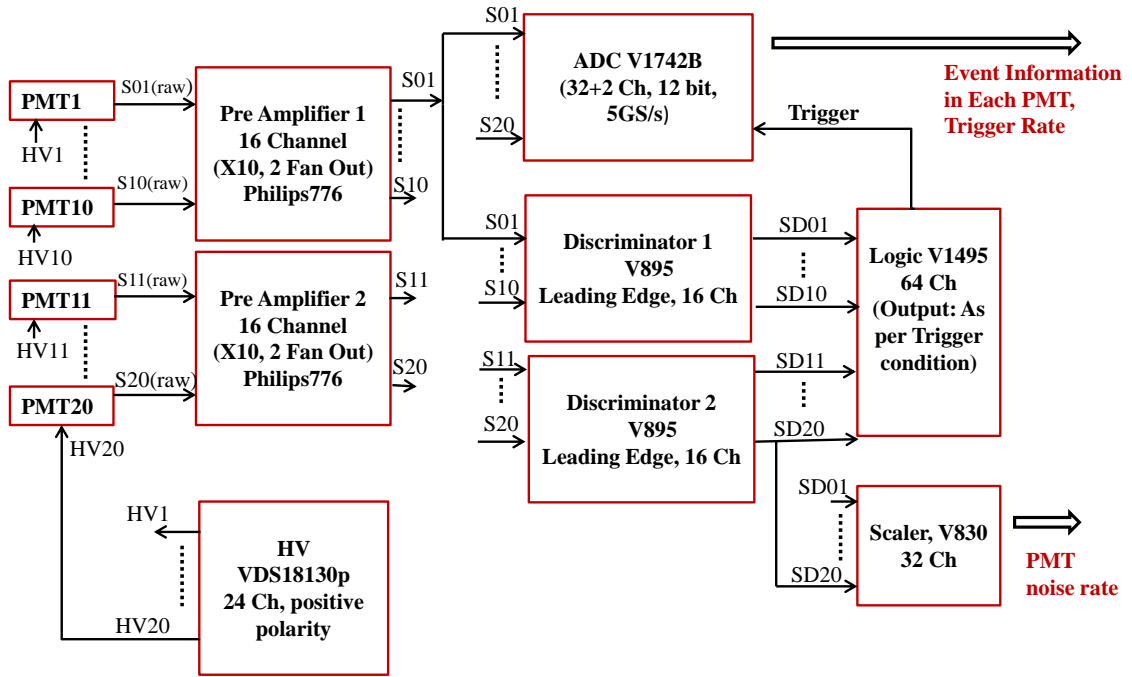
[6] CAEN V830

Figure 9. The schematic of the Data Acquisition System of DIREXENO. It consists of 20 PMTs and the subsequent electronic channels to record the events for an internal trigger generated by the coincidence of any two PMTs in the system and also the PMT noise rate.

4 Simulation

In this section we present the Monte Carlo simulation study that was performed to optimize the geometry and performance of the LXe scintillation detection system. We perform a GEANT4 based simulation to obtain the reasonable dimensions of the spherical LXe holder and the placement of the PMT detectors around it, which is described in section 4.1. In section 4.2, we discuss the statistical test performed to find the detector's sensitivity in measuring various patterns of the scintillation emission from the LXe target.

4.1 The Detector Geometry

We perform a study to optimize the dimensions of the setup using a GEANT4 based framework that includes realistic description of the target, the enclosing HPFS sphere and the PMTs around. The simulations takes into account the physics processes of the propagation of the photons from the LXe target through the the sphere and the vacuum and their interaction at the PMTs. The parameters under test for this study are the size of the sphere, the PMT size and their placement around the sphere. The refractive index and internal transmittance of both of LXe and of HPFS are known with good precision.

For the simulation, we fix all parameters except the outer radius (R_2) of the sphere. The fixed parameter values are chosen by quantitative physical considerations and educated guesses. The radius of the LXe target R_1 will determine the event rate for a particular source, and we choose it to be 1 cm. The conventional PMTs designed by Hamamatsu to detect scintillation from LXe are 1" and 3" square PMTs, and we choose the 1' ones in order to get better spatial resolution. an array of 20 PMTs around the sphere, placed at a distance of 39 mm from the centre of the targetare considered. The active area of each PMT is 22 mm × 22 mm.

Table 1. The optical parameters used in simulation

Parameter	Value
LXe absorption length	100 cm
LXe scattering length	35 cm
HPFS absorption length	100 cm
HPFS scattering length	∞
LXe refractive index	1.61
HPFS refractive index	1.57

In order to chose a reasonable dimension of the sphere, we first study the detection efficiency of scintillated photons in the simulated setup. Using an inotropic emmision of 50photons/event, we find the average ratio of the detected photons/event to the net emitted photons/event, for various choices of R_2. The trasmittance of HPFS is a crucial parameter and we vary it within a large range to check the impact of it. The photon detection ratio for different sets of R_2 and transmittance are shown in Fig. 10. At very low R_2 the total internal reflections causes the number of photons emerging from the sphere to drop. As the R_2 increases the total internal reflections decreases resulting in an increase in the number of photons croosing the sphere. After certain increase in

Figure 10. The photon detection ratio as a function of R_2, for different transmittances of the fused silica shell. We use 10^4 events with 50 photons/event for each choice of transmittance and R_2. At very low R_2 the total internal reflections causes the number of photons emerging from the sphere to drop. As the R_2 increases the total internal reflections decreases resulting in an increase in the number of photons croos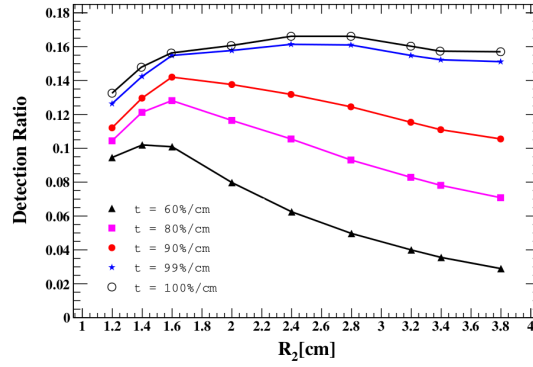ing the sphere. After certain increase in R_2, the transmittance of HPFS becomes the dominant factor and the photon detection ratio starts falling.

R_2, the transmittance of HPFS becomes the dominant factor and the photon detection ratio starts falling. This is an important factor to chose a suitable value of R_2.

4.2 The statistical test

In this section, we present the study on the ability of the proposed detector to detect the emission pattern of the LXe scintillation with a high statistical significance. For each scintillation event, the PMTs will detect only a certain fraction of the total photons produced. We pick a few cases of emission patterns as shown in Table 2,

Table 2. The emission patterns used in simulation

Pattern no.	Beam specification	Beam Half widths	Signal fractions
LXe absorption length	100 cm		
LXe scattering length	35 cm		
HPFS absorption length	100 cm		
HPFS scattering length	∞		
LXe refractive index	1.61		
HPFS refractive index	1.57		

5 Summary

References

[1] E. Aprile and T. Doke. Liquid Xenon Detectors for Particle Physics and Astrophysics. *Rev. Mod. Phys.*, 82:2053–2097, 2010.

[2] A. Rubbia. Future liquid Argon detectors. 2013. [Nucl. Phys. Proc. Suppl.235-236,190(2013)].

[3] J. Silk et al. *Particle Dark Matter: Observations, Models and Searches*. Cambridge Univ. Press, Cambridge, 2010.

[4] E. Aprile et al. First Dark Matter Search Results from the XENON1T Experiment. 2017.

[5] D. S. Akerib et al. Results from a search for dark matter in the complete LUX exposure. *Phys. Rev. Lett.*, 118(2):021303, 2017.

[6] Changbo Fu et al. Spin-Dependent Weakly-Interacting-Massive-ParticleâĂŞNucleon Cross Section Limits from First Data of PandaX-II Experiment. *Phys. Rev. Lett.*, 118(7):071301, 2017.

[7] J. Aalbers et al. DARWIN: towards the ultimate dark matter detector. *JCAP*, 1611:017, 2016.

[8] R. H. Dicke. Coherence in spontaneous radiation processes. *Phys. Rev.*, 93:99–110, Jan 1954.

[9] M. Gross and S. Haroche. Superradiance: An essay on the theory of collective spontaneous emission. *Physics Reports*, 93(5):301 – 396, 1982.

[10] N G Basov, V A Danilychev, and Yurii M Popov. Stimulated emission in the vacuum ultraviolet region. *Soviet Journal of Quantum Electronics*, 1(1):18, 1971.

[11] Frederick H. Mies. Stimulated emission and population inversion in diatomic bound-continuum transitions. *Molecular Physics*, 26(5):1233–1246, 1973.

[12] K L Giboni, X Ji, H Lin, A Tan, T Ye, Y Zhang, and L Zhao. A liquid xenon development and test system. *Journal of Instrumentation*, 9(04):T04006, 2014.

[13] E. Aprile et al. The XENON100 Dark Matter Experiment. *Astropart. Phys.*, 35:573–590, 2012.

[14] S. Agostinelli et al. GEANT4: A Simulation toolkit. *Nucl. Instrum. Meth.*, A506:250–303, 2003.